Performance Characteristics of an Injection-Controlled Electron-Beam Pumped XeF($C \rightarrow A$) Laser System

NAOYA HAMADA, ROLAND SAUERBREY, MEMBER, IEEE,
WILLIAM L. WILSON, JR., SENIOR MEMBER, IEEE,
FRANK K. TITTEL, FELLOW, IEEE, AND
WILLIAM L. NIGHAN, SENIOR MEMBER, IEEE

Abstract—Characteristics of an injection-controlled electron-beam pumped XeF($C \rightarrow A$) laser have been investigated with emphasis on *efficient* wide-band tuning and scaling issues. Using a quasi-CW dye laser as an injection source, data were obtained that describe the laser characteristics over a wide parameter range. A high Z electron-beam backscattering reflector inside the laser reaction cell improved the electron-beam energy deposition by 40 percent, resulting in an increase of the amplified laser output by more than a factor of four. *Efficient* and *continuous* wavelength tuning between 470 and 500 nm has been achieved with an output energy density of ~1 J/l, and an intrinsic efficiency of ~1 percent throughout the entire tuning region.

I. INTRODUCITON

AN efficient, electrically excited high-power laser with wide-band and continuous wavelength tuning characteristics in the visible spectral region is a desirable optical source for many diverse applications ranging from optical communications to laser spectroscopy. The XeF($C \rightarrow A$) excimer transition exhibits an exceptionally broadband fluorescence spectrum in the blue–green, and has the potential to meet such laser requirements. Free-running stable laser oscillators operating on the XeF($C \rightarrow A$) transition typically exhibit a broad laser spectrum (~20 nm, FWHM) centered near 485 nm [1]. Such an XeF($C \rightarrow A$) laser has also been tuned from about 450 to 510 nm with a spectral width on the order of a few nanometers, albeit with very low efficiency [2]–[4]. More recently, efficient and narrow spectral width (0.001–0.01 nm) operation of the XeF($C \rightarrow A$) laser has been achieved for wavelengths near 480 nm by using injection-control [5], [6]. In that work, the tuning was neither continuous nor efficient, due in part to the presence of transient absorbing species [7] which give rise to broadband absorption and to narrow line absorption corresponding to transitions in the rare-gas atoms. The very high saturation intensity (>

10^6 W/cm^2) of the XeF($C \rightarrow A$) transition, due primarily to its small stimulated emission cross section (~10^{-17} cm^2), indicated, however, that the transient absorption might be saturable through the use of a strong injection photon flux [8].

Our previous work [6] was hampered by a limited database because of the uncertainty between the timing of the injection laser pulse and the electron-beam pulse, each having a temporal duration of approximately 10 ns, a value less than the inherent jitter of the electron-beam generator (~50 ns). Also, in those studies, the electron-beam energy deposition in the laser cell was kept constant. Thus, the relationship among excitation rate, small-signal gain, and laser output was not completely characterized. It is important that these relationships be understood in order to realize higher output energy levels and/or higher efficiency through system scaling.

This paper describes the following new experimental results: 1) injection control of an XeF($C \rightarrow A$) laser using a long pulse quasi-CW injection source, 2) *efficient* and *continuous* tuning over a 30 nm wavelength range, 3) scaling of the injection-controlled XeF($C \rightarrow A$) laser performance with pumping power, and 4) initial geometric scaling of the XeF($C \rightarrow A$) laser.

The details of the experimental arrangement and related diagnostics are described in Section II. In Section III, experimental results are presented along with a discussion of prospects for further improvement in XeF($C \rightarrow A$) laser performance.

II. EXPERIMENT

A. Electron-Beam Excitation System and Reaction Cell

The experimental setup used in this study is shown in Fig. 1. A Physics International Pulserad 110 electron-beam generator was used to transversely excite the high-pressure laser gas mixture through a metal foil. The electron-beam energy was 1 MeV, and the excitation pulse duration was 10 ns (FWHM). In order to obtain a maximum foil lifetime, a stainless steel wire mesh was mounted as an anode between the electron-beam cathode and the foil. The electron-beam cathode length used for most of the experiments was 7.6 cm. A 15.2 cm long
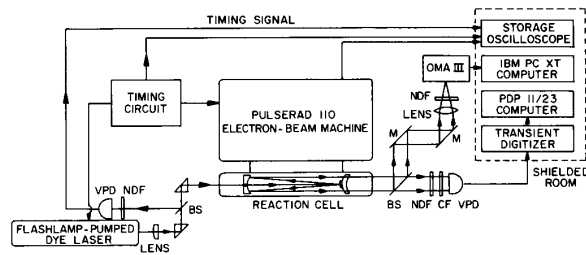
Fig. 1. Schematic illustration of the experimental setup, showing the unstable cavity optics inside the reaction cell, the tunable injection laser, and the timing and data acquisition systems. OMA: optical multichannel analyzer, VPD: vacuum photodiode, CF: color glass filter, NDF: neutral density filter, BS: beam splitter, M: total reflection mirror.
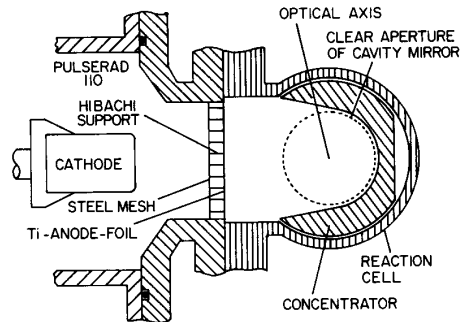
Fig. 2. Schematic representation of a transverse section of the electron-beam pumping region with the concentrator in place.

cathode was used in order to investigate the scaling of the laser output with increased pumping length. To vary the electron-beam excitation level of the laser gas mixture, various foil conditions and anode–cathode spacing values were employed. Typically, a 50 μm nickel-plated titanium foil was used. In order to reduce the electron-beam energy deposition, a 50 μm inconel foil was also employed in some of the experiments. Due to the higher atomic number of inconel compared to titanium, the scattering angle of the electrons passing through the foil is increased, resulting in a reduced energy deposition. Therefore, a combination of foils was adopted for further reduction of the energy deposition. It is possible to achieve a 40 percent energy reduction with an inconel foil, and a 65 percent energy reduction with a combination of both foils compared to the energy deposition value obtained using only a titanium foil. In addition, the anode–cathode spacing in the electron-beam diode could be changed in order to vary the current density available inside the laser cell.

Improved electron-beam energy deposition was achieved by means of an electron-beam backscattering reflector or so-called *concentrator* [9]. The concentrator was made of lead in order to obtain good backscattering of the electron beam. Its inner shape was concentric with the cavity optical axis surrounding the active volume as illustrated in Fig. 2. To avoid chemical reactions between lead and fluorine, the concentrator was nickel plated. The thickness of the nickel plating was about 1 μm, which is small compared to the typical penetration depth of 1 MeV electrons in nickel or lead. Therefore, the backscattering behavior of the device is governed by the high atomic number of lead and not by the surface material.

Current density values on the optical axis (2.3 cm from the foil) at an argon pressure of 6.5 atm were measured without the concentrator using a Faraday cup probe. The peak current density varied from ~ 100 to ~ 290 A/cm^2, depending upon the foil material and the anode–cathode spacing. The energy deposition into the laser medium with the concentrator in place was measured on the optical axis using chlorostyrene film [10]. The deposition value was obtained by measuring the optical density of the irradiated film with an He–Ne laser. The dynamic range of these films extends over more than two orders of magnitude.

The average energy deposition density over the active pumping length along the optical axis, estimated to be ~ 10 cm, ranged from ~ 37 to ~ 112 J/l, depending upon which electron-beam coupling foil was used.

High-purity research grade laser gases (NF$_3$, He–10 percent F$_2$, Xe, Kr, and Ar) were used as source materials. The typical gas composition was 8 torr NF$_3$, 1 torr F$_2$, 8 torr Xe, 300 torr Kr, and 6.1 atm Ar, for a total pressure of ~ 6.5 atm [6], [7], [11]. Good mixing of the different gas components was achieved by rapid turbulent flow as each high-pressure gas component was introduced into the reaction cell. Each fresh gas mixture could be used for about ten shots without significant degradation of the laser performance. Nickel plating of the concentrator and the titanium foil considerably increased the lifetime of the laser gas mixture, and contributed to the reproducibility of the experiments. This will be of particular importance in scaled versions of this laser that require gas flow systems. The stainless steel reaction cell and the concentrator were well passivated by prolonged exposure to fluorine prior to any experiments.

B. Injection-Control System

The aforementioned timing uncertainty in earlier experiments between the injection laser pulse and firing of the electron beam was eliminated by replacing the 10 ns excimer-pumped dye laser used previously [6], with a long pulse (250 ns) coaxial flashlamp-pumped dye laser. A Phase-R dye laser system (DL-1200VT) having a spectral width of ~ 0.6 nm was used as the injection laser. Operated with an LD490 dye, the system can deliver an output pulse of ~ 40 mJ over the 470–500 nm wavelength range, in a 250 ns pulse (FWHM), with a beam diameter of 2.6 mm and beam divergence of ~ 1.5 mrad. The long pulse duration of this laser ensured good temporal overlap of the injection signal and electron-beam firing. A 1 m focal length plano-convex lens was used to reduce the injection beam diameter from 2.6 to 1.5 mm so that most of the available dye laser pulse energy entered the unstable resonator located inside the reaction cell (Fig. 1). A beam splitter on the injection optical axis allowed observation of the backreflected beam from the laser cavity using a fast vacuum photodiode detector (Hamamatsu R1193U-03). Due to the low damage threshold of the optics coat-

ings used in the present investigation, the energy of the injected signal was limited to a maximum value of ~ 5 mJ (~ 0.3 J/cm^2).

C. Diagnostics

The temporal evolution of the free-running laser (without injection), the dye laser throughput, and the injection-controlled XeF($C \to A$) laser output were monitored using a fast vacuum photodiode detector (ITT F4000(S5)). Neutral density filters were used to avoid saturation of the photodiode, and a color glass filter was used to define the spectral region of interest. Signals were recorded by a Tektronix R7912AD transient digitizer. The time resolution of the system was better than 2 ns. For an absolute energy measurement, this system was calibrated with the dye laser and a pyroelectric energy detector (Gentec ED-200). As a further check of the calibration procedure, the XeF($C \to A$) laser output energy was sometimes directly measured by the pyroelectric energy detector. With this system, we estimate the absolute accuracy of the measured laser energy to be ±20 percent.

The temporally integrated, spectrally resolved laser output was recorded by an optical multichannel analyzer (OMAIII), using a Jarrell–Ash 0.25 m spectrometer with a spectral resolution of about 0.45 nm. The temporal relationship of the dye laser and electron-beam pulse was monitored by a photodiode–storage oscilloscope combination (Fig. 1).

D. Cavity Optics

The optical cavity used in this study was a positive-branch confocal unstable, intracell resonator, consisting of a concave end mirror with an injection hole of 1.5 mm diameter and a coating having a high reflectivity in the blue–green region, and a convex output coupler (Fig. 1). The role of the cavity was to serve as a beam expanding telescope for a regenerative amplifier [5], [12]. The mirrors, having focal length of f_2 and $-f_1$, respectively, were separated by a distance $L = f_2 - f_1$. The cavity lengths used, $L = 12.5$ cm and $L = 18$ cm, correspond to electron-beam cathode lengths of 7.6 and 15.2 cm, respectively. The magnification of the unstable resonator is given by $M = f_2/f_1$. Various cavities were examined with magnifications of 1.05, 1.08, 1.15, and 1.23 for the 12.5 cm long cavity. A resonator with $M = 1.15$ yielded optimum laser output energy under conditions of high excitation and injection, and was adopted as a standard value. The output coupler was a meniscus lens of zero refraction power having a highly reflective coating spot on the convex side with a diameter $d = 1.4$ cm for $L = 12.5$ cm and $d = 1.5$ cm for $L = 18$ cm. The active region was a cylindrical volume defined by the electron-beam pumping length (~ 10 cm) and a clear aperture having a diameter $d \times M$, i.e., ~ 0.02 l for typical operating conditions.

E. Gain Measurement

The experimental arrangement for measuring the gain was similar to that shown in Fig. 1. However, in this case,
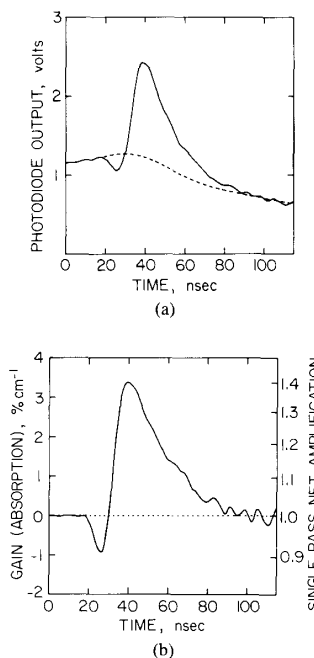
Fig. 3. Temporal evolution of the transmitted probe laser pulse at 478.6 nm (a), and of the XeF($C \to A$) net gain profile (b). The mixture was comprised of 8 torr NF$_3$, 1 torr F$_2$, 8 torr Xe, 300 torr Kr, and 6.1 atm Ar, and the *average* energy deposition of the electron beam for this condition was 95 J/l. The dashed line in Fig. 3(a) refers to the transmitted probe laser when the electron beam is not fired.

the dye laser was used as a probe laser. The laser intensity was attenuated appropriately for small-signal gain measurement, and then increased in order to investigate gain saturation, while 1 m focal length lens in Fig. 1 was taken out to avoid early gain saturation. The probe beam diameter at the cell was 4 mm. For these experiments, the concave end mirror was removed and the output coupler was replaced with a flat total reflector creating a double path for the probe beam through the cell. The temporal profile of the backreflected probe laser was monitored using the fast vacuum photodiode.

During the dye laser pulse duration (250 ns, FWHM), gain occurs only when the electron beam is fired. Fig. 3(a) shows a typical temporal profile on the transmitted probe laser pulse measured with this arrangement, indicating a superposition of a *portion* of the total dye laser pulse and the laser absorption/gain characteristic. In order to interpret this profile, the temporal pulse shape of the dye laser has to be determined as shown by the dashed line in Fig. 3(a). By taking the logarithm of the ratio of the laser pulse with and without gain at various times, and dividing by twice the electron-beam pumping length, the temporal gain profile was obtained as shown in Fig. 3(b). Due to the uncertainty of the dashed line fitting in Fig. 3(a), the value of Fig. 3(b) has an uncertainty of ~ ±0.2 percent/cm. Although there is a slight uncertainty in the determination of the temporal pulse shape of the dye laser, this method permits flexible gain measurements at any wavelength of interest and at any intensity level.

III. EXPERIMENTAL RESULTS AND DISCUSSION

A. Electron-Beam Energy Deposition and Its Effect

In order to study the effect of the concentrator on electron-beam energy deposition, several parameters were investigated. The energy deposited into the laser gas mixture was determined with and without the concentrator. Laser gain and injection-controlled laser output measurements were also performed with and without the concentrator in place. Fig. 4 shows the electron-beam energy deposition measured using overlapping 7.0 × 1.6 cm chlorostyrene film strips [10]. Electron-beam energy deposition in the cell was measured on the optical axis for an argon pressure of 6.5 atm. This figure shows that the electron-beam deposition profile is not uniform along the optical axis, but strongly peaks at the center of the cell. Due to this inhomogeneity, the electron-beam energy deposition in the optical volume must be averaged. The procedure should include three-dimensional averaging, that is, along the cavity axis, along the vertical direction, and along the horizontal orientation of Fig. 2. By positioning the film strips at various locations in the active volume, it was found that the average value in the vertical plane including the optical axis represents the average energy deposition over the total volume. Thus, *average* energy deposition was determined in this manner.

The average length along the optical axis is taken to be 10 cm, which is the effective aperture length defined by the spacing between the cavity mirror holders. Consequently, the gain characteristic shown in Fig. 3 is the spatially *averaged* profile over the inhomogeneous pumping length. We estimate that the absolute gain coefficient may have a relative error of ~20 percent due to the uncertainty of this averaging procedure. Since the gain is a nonlinear function of the pumping energy, the gain spatial distribution will be different from that shown in Fig. 4. Indeed, both experiments and modeling show that, *for our conditions*, the gain saturates for pumping densities over 100 J/l. With the concentrator in position, the energy deposition in the center of the cell exceeds 100 J/l (Fig. 4). Thus, the spatial inhomogeneity of the gain profile is expected to be significantly less than that exhibited by the electron-beam pumping profile. For the specific conditions of Fig. 4, the average energy deposition densities over the 10 cm pumping length with and without the concentrator were 95 and 68 J/l, respectively.

1) Gain: The effect of the concentrator on the *peak* gain (Fig. 3) is shown in Fig. 5 as a function of the power density of the probe laser. Gain was measured on the optical axis at a wavelength of 478.6 nm for which the gain is close to its maximum value [6]. The error bar shown in the figure refers to shot-to-shot variations. At low injected powers, the peak gain coefficient is about 3.0 and 3.4 percent/cm without and with the concentrator, respectively, decreasing to values of about 2.6 and 3.0 percent/cm at higher injection powers. These data show an increase in peak gain of only ~15 percent, corresponding to an in-
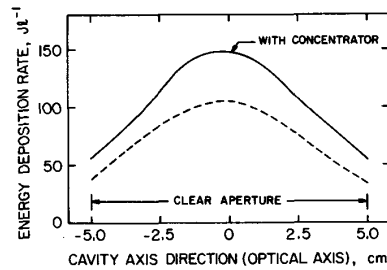
Fig. 4. Electron-beam energy deposition spatial profiles on the optical axis (2.3 cm from the foil) with and without the concentrator for an argon pressure of 6.5 atm. The electron-beam cathode length was 7.6 cm, and the coupling foil was 50 μm titanium. For this condition, the *average* energy deposition density was 68 and 95 J/l, without and with the concentrator.
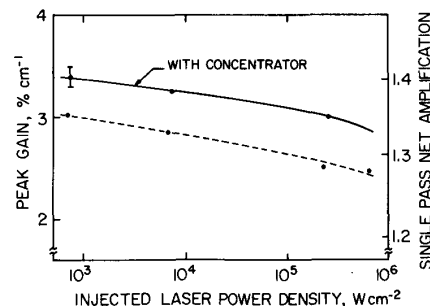
Fig. 5. Comparison of *peak* gain with and without the concentrator at a wavelength of 478.6 nm for a mixture comprised of 8 torr NF_3, 1 torr F_2, 8 torr Xe, 300 torr Kr, and 6.1 atm Ar. The solid line refers to the peak gain with the concentrator in place, corresponding to *average* energy deposition of 95 J/l, while the dashed line corresponds to 68 J/l (no concentrator).

crease in average energy deposition from 68 to 95 J/l, i.e., ~40 percent. This is a reflection of the onset of the gain saturation as the energy deposition of our 10 ns pulse approaches ~100 J/l. Kinetic modeling indicates that this effect is due primarily to electron quenching of XeF(B, C), which becomes more important as the electron-beam pumping density, and therefore the electron density, increases.

2) Laser Output Energy: Fig. 6 shows the output energy of the injection-controlled XeF($C \rightarrow A$) laser as a function of the injection power. Injection input was defined by the power density at the 1.5 mm diameter hole of the concave cavity mirror. Also shown for comparison is the energy injected during the ~10 ns period when gain is rising (Fig. 3). At a 1 MW/cm² dye laser input level, the output energy increased by a factor of 4 when the concentrator was used, a reflection of the higher gain (Fig. 5). At the lower injection energy, the increase was even greater since the medium was not saturated. Since the effect of the concentrator was quite dramatic, resulting in a higher energy deposition, higher gain, and therefore larger XeF($C \rightarrow A$) laser output energy, the concentrator was utilized in all of the experiments reported below.
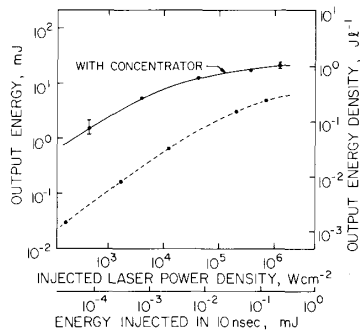
Fig. 6. XeF($C \rightarrow A$) output energy dependence on the injected dye laser power at 478.6 nm with the concentrator (solid line) and without the concentrator (dashed line) using a cavity magnification value of $M = 1.15$.

B. Pump Energy Variation

In order to optimize the intrinsic efficiency and absolute output energy of the laser, the relationship between the pumping power density and laser output must be understood. In order to study this, the electron-beam energy deposition was varied, mainly by altering the composition of the coupling foil as described in Section II-A. Gain and laser output at various injection energy levels were then studied as a function of pumping energy. Fig. 7 shows the dependence of the peak gain at 478.6 nm on electron-beam energy deposition for injection power densities of 350 W/cm^2 and 350 kW/cm^2, the latter value approximately 10 percent of the saturation intensity. This figure shows the strong dependence of the peak gain on pumping energy, especially for the lower values of the latter. The peak gain tends toward saturation at the higher pumping level as was discussed previously.

The dependence of laser output and intrinsic efficiency on the electron-beam pumping level for a dye laser power density of 360 kW/cm^2 (64 μJ in 10 ns) is shown in Fig. 8. For these conditions, the cavity magnification was 1.15, and the injection wavelength was 478.6 nm. Fig. 8 shows typical laser amplification characteristics. Although a high injection power density is applied, there is a linear relationship between pumping power and laser output for low pumping powers, which saturates at higher pumping levels due to the peak gain saturation shown in Fig. 7. With regard to the intrinsic efficiency plotted in the figure, the spatially averaged excitation level of ~ 90 J/l was found to be optimum.

C. Geometric Scaling

In order to consider system scaling to achieve higher energy output, it is also important to understand the relationship between pumped volume and laser output. For scaling considerations, it is of particular importance to determine whether the laser output scales with active length and what is the optimum length for an XeF($C \rightarrow A$) amplifier. For this reason, a second pumping length was selected using a 15.2 cm long electron-beam cathode.
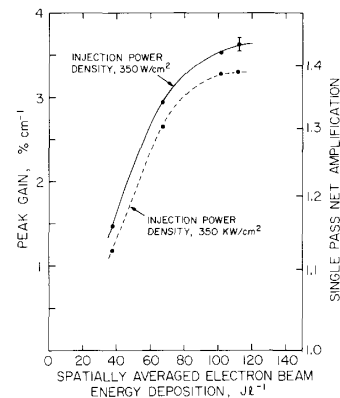
Fig. 7. Peak gain dependence on the electron-beam energy deposition at 478.6 nm for injection power density of 350 W/cm^2 (solid line, 440 nJ in 10 ns) and 350 kW/cm^2 (dashed line, 440 μJ in 10 ns).
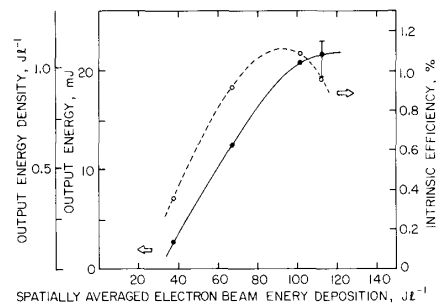
Fig. 8. Laser output and intrinsic efficiency dependence on the electron-beam pumping level at 478.6 nm using a cavity magnification value of $M = 1.15$. Injected laser power density is 360 kW/cm^2 (64 μJ in 10 ns). The solid line shows the output energy, while the dashed line represents the intrinsic efficiency.

The effective pumping length based on energy deposition measurements (Section III-A) was found to be 17.5 cm, and the average value of the energy deposition was 37 J/l, which was the same as the lowest pumping level obtained with the 10 cm pumping length. Increased energy deposition at this longer cathode length was impossible due to electron-beam machine design limitations. Injection-controlled laser experiments were conducted using an $M = 1.15$ cavity as a function of injection power density at 478.6 nm wavelength. Fig. 9 depicts the comparison of laser output characteristics for 10 and 17.5 cm pumping lengths for the same pumping level. The results are plotted in terms of the output energy densities as a function of the injection energy level in order to make a consistent comparison. Absolute energy outputs are also shown on the right side scales of the figure. At the low injection energies, the output energy density is almost one order of magnitude larger for the 17.5 cm pumping length, reflecting the exponential dependence of the small-signal amplification on length, whereas output energy density values approach each other with increasing injection power. This result indicates that with increased pumping length,
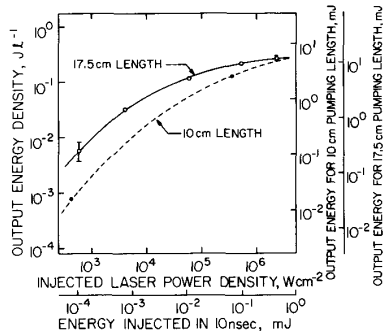
Fig. 9. Geometric scaling effect for a same electron-beam pumping level of 37 J/l; the injection wavelength was 478.6 nm and the cavity magnification was 1.15. The solid line represents the laser outputs for 17.5 cm pumping length, while the dashed line corresponds to a 10 cm pumping length.

Fig. 10. Free-running XeF ($C \rightarrow A$) laser spectrum. Specific wavelengths for the tuning experiments are indicated.

the output energy scales with the pumping length even for the saturated region. The relatively low output energy density value in the saturated region is simply due to the low electron-beam pumping level (37 J/l).

D. Wavelength Tuning

An investigation of wavelength tuning efficiency was conducted by measuring the peak gain and the laser output as a function of the dye laser injection intensities. The electron-beam cathode length and the cavity length were again set at 7.6 and 12.6 cm, respectively, for these experiments. The specific injection wavelengths were chosen to correspond to either the gain maxima or the absorption valleys that are always apparent in the free-running XeF($C \rightarrow A$) laser spectrum as shown in Fig. 10. The shape of the free-running laser spectrum is governed by the coating bandwidth of the cavity mirrors used in this investigation (470–500 nm), by wide-band absorption due primarily to photoionization of excited Xe atoms [1], and by discrete narrow-band absorption which is due mainly to phototransitions of Xe, Ar, and Kr excited atoms [1], [13]. Because of the bandwidth limitation of the cavity optics coatings, the tuning range of the injection dye laser was restricted to wavelengths between 470 and 500 nm, a region where the gain is relatively insensitive to wavelength [6], except for specific wavelengths at which discrete absorption occurs.

1) Gain: Gain measurements were performed at two maxima and two valley wavelengths as a function of the probe beam intensity as shown in Fig. 11. The spatially averaged electron-beam pumping density was 95 J/l. Wavelengths of 478.6 and 486.8 nm correspond to the gain maxima positions, whereas those of 481.2 and 483.5 nm are valley positions (Fig. 10). Fig. 11 shows that with increasing injection power, the gain at the wavelength maximum locations decreases, whereas in the valley positions, the gain actually *increases*. As previously discussed, the measured gain is an average over a very inhomogeneous pumping power distribution (Fig. 4); therefore, these data have primarily qualitative significance. The decrease of the gain at 478.6 and 486.8 nm as
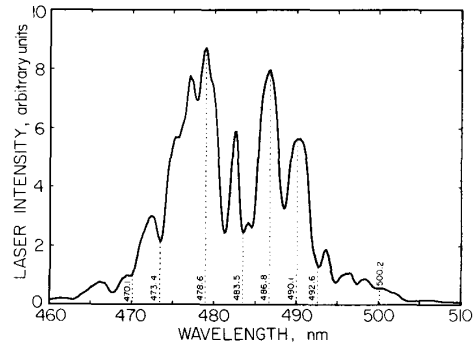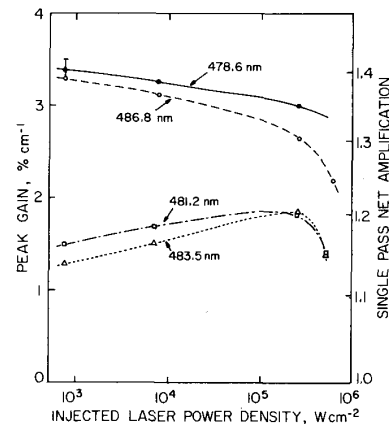
Fig. 11. Peak gain dependence on injected power density of the probe laser beam at various discrete wavelengths (Fig. 10); the electron-beam pumping energy was 95 J/l.

the injected power increases is most likely due to saturation of the gain over at least a portion of the gain length. At the 481.2 and 483.5 nm valleys where discrete absorption dominates, the increase in gain as the injected power increases suggests that absorber bleaching becomes important before the gain saturates.

2) Laser Energy: Presented in Fig. 12 are measured output energy characteristics as a function of wavelength for injection power density values of 430 W/cm^2 (76 nJ in 10 ns) and 360 kW/cm^2 (64 μJ in 10 ns). The spatially averaged electron-beam pumping level was 112 J/l. Each figure shows the superposition of the spectra of several *separate* injection-controlled laser shots. The line widths of the measured laser spectra were identical to those of the injected dye laser as previously reported [6]. Each spectrum shows relatively broad line width (0.75 nm). This is due to the convolution of the orginal dye laser line width (~0.6 nm) and the spectral resolution of the measuring system (~0.45 nm).

When a comparatively small power of 430 W/cm^2 was injected, the laser operated in the unsaturated region where the peak gain is high at gain maxima wavelength values and low at valley positions. Thus, the tuning data of Fig.
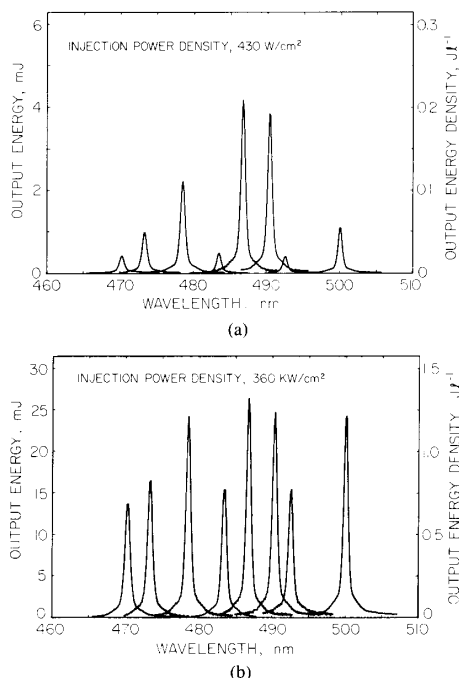
Fig. 12. Amplified XeF($C \rightarrow A$) laser output for various injection laser wavelengths and injection power densities of (a) 430 W/cm^2 (76 nJ in 10 ns), and (b) 360 kW/cm^2 (64 μJ in 10 ns).

12(a) exhibit characteristics qualitatively similar to those of the free-running spectrum. However, when a relatively high power was injected, 360 kW/cm^2, the tuned output shows a very significant change as depicted in Fig. 12(b). At the higher injection power level, the valleys become very much less pronounced, i.e, the wavelength tuning curve becomes flatter. This is apparently due to the bleaching of the absorbers which is in agreement with the gain measurements of Fig. 11. In fact, for low power injection, the output energy variation over a 30 nm region was a factor of 10. However, only a factor of 2 variation was observed with higher power injection.

For the conditions of Fig. 12(b), the *minimum* measured energy output of 14 mJ at 470.1 nm corresponds to an output energy density of 0.7 J/l, and an intrinsic efficiency of 0.6 percent, while the maximum measured energy output of 26 mJ at 486.8 nm corresponds to 1.3 J/l and 1.15 percent, respectively. It should be emphasized that these values refer to an injection power density of 360 kW/cm^2, and are not maximum values. When 1.1 MW/cm^2 was injected at a wavelength of 486.8 nm, which exhibited the maximum output at 360 kW/cm^2, an output energy of 33 mJ was obtained corresponding to an energy density of 1.6 J/l and an intrinsic efficiency of 1.5 percent.

IV. SUMMARY

The results of this investigation provide encouraging evidence that the electrically excited XeF($C \rightarrow A$) me-

dium has significant potential for the development of an *efficient* optical source that is *continuously* tunable throughout most of the blue–green spectral region. In addition, they provide the criteria for the efficient operation of this laser as a high-power excimer laser. Geometrical scaling confirms that the output energy scales with the pumping length.

Although relatively efficient (~ 1 percent) tuning has been demonstrated for wavelengths between 470 and 500 nm, XeF($C \rightarrow A$) amplifier performance has been limited in the present investigation by the combination of a relatively low damage threshold and the bandwidth of the cavity mirror coatings, a short active length (~ 10 cm), and an undesirably low value of cavity magnification (M = 1.15) which was required to compensate for the short active length and low stimulated emission cross section. However, it is clear that these factors are not fundamental limitations. For example, the present damage threshold of ~ 0.3 J/cm^2 is far below the current state of the art (few J/cm^2) even if the cavity optics are exposed to fluorine-containing gas mixtures. Considering the relatively high gain and the absorber bleaching effect at the absorption valleys, significant improvement in laser performance throughout the entire blue–green region (~ 450–520 nm) should be possible by realizing improved resonator optics and by scaling of the laser medium excitation volume, assisted by magnetic field electron-beam confinement.

REFERENCES

[1] Y. Nachshon, F. K. Tittel, W. L. Wilson, Jr., and W. L. Nighan, "Efficient XeF($C \rightarrow A$) laser oscillation using electron-beam excitation," *J. Appl. Phys.*, vol. 56, pp. 36–48, 1984.

[2] W. K. Bischel, D. J. Eckstrom, H. C. Walker, Jr., and R. A. Tilton, "Photolytically pumped XeF($C \rightarrow A$) laser studies," *J. Appl. Phys*, vol. 52, pp. 4429–4434, 1981.

[3] C. H. Fisher, R. E. Center, G. J. Mullaney, and J. P. McDaniel, "Multipass amplification and tuning of the blue–green XeF($C \rightarrow A$) laser," *Appl. Phys. Lett.*, vol. 35, pp. 901–903, 1979.

[4] G. Marowsky, N. Nishida, F. K. Tittel, W. L. Wilson, Jr. and Y. Zhu, "Wideband tuning of the blue–green XeF($C \rightarrow A$) laser," *Appl. Phys. B.*, vol. 37, pp. 205–207, 1985.

[5] G. Marowsky, N. Nishida, H. Stiegler, F. K. Tittel, W. L. Wilson, Jr., Y. Zhu, and W. L. Nighan, "Efficient narrow spectral output in the blue–green region from an injection-controlled electron-beam excited XeF($C \rightarrow A$) laser," *Appl. Phys. Lett.*, vol. 47, pp. 657–660, 1985.

[6] F. K. Tittel, G. Marowsky, W. L. Nighan, Y. Zhu, R. Sauerbrey, and W. L. Wilson, Jr., "Injection-controlled tuning of an electron-beam excited XeF($C \rightarrow A$) laser," *IEEE J. Quantum Electron.*, vol. QE-22, pp. 2168–2173, 1986.

[7] W. L. Nighan, R. Sauerbrey, Y. Zhu, F. K. Tittel, and W. L. Wilson, Jr., "Kinetically tailored properties of electron-beam excited

XeF($C \rightarrow A$) and XeF(B $\rightarrow$ X) laser media using an Ar–Kr buffer,'' *IEEE J. Quantum Electron.*, vol. QE-23, pp. 253–261, 1987.

[8] Y. Nachshon and F. K. Tittel, "A new blue–green XeF($C \rightarrow A$) excimer laser amplifier concept," *Appl. Phys. B*, vol. 35, pp. 227–231, 1984.

[9] R. Sauerbrey, Y. Zhu, P. Millar, F. K. Tittel, and W. L. Wilson, Jr., "Improved laser pumping by intense electron beams via a back-scattering reflector," *J. Appl. Phys.*, vol. 61, pp. 4740–4743, 1987.

[10] W. P. Bishop, K. C. Humpherys, and P. T. Randtke, "Poly(halo)styrene thin-film dosimeters for high doses," *Rev. Sci. Instrum.*, vol. 44, pp. 443–452, 1973.

[11] W. L. Nighan, F. K. Tittel, W. L. Wilson, Jr., N. Nishida, Y. Zhu, and R. Sauerbrey, "Synthesis of rare gas-halide mixtures resulting in efficient XeF($C \rightarrow A$) laser oscillation," *Appl. Phys. Lett.*, vol. 45, pp. 947–949, 1984.

[12] I. J. Bigio and M. Slatkine, "Injection locking unstable resonator excimer lasers," *IEEE J. Quantum Electron.*, vol. QE-19, pp. 1426–1436, 1983.

[13] H. Horiguchi, R. S. F. Chang, and D. W. Setser, "Radiative lifetimes and two-body collisional deactivation rate constants in Ar for Xe($5p^56p$), Xe($5p^56p$) and Xe($5p^57p$) states," *J. Chem. Phys.*, vol. 75, pp. 1207–1218, 1981.

Naoya Hamada was born in Tokyo, Japan, on February 26, 1957. He received the B.S. degree in 1979 and the M.S. degree in 1981 from the University of Tokyo, Tokyo, Japan, and the Ph.D. degree in 1988 from Rice University, Houston, TX.

Since 1981, he has been a Research Scientist at Nippon Steel Corporation, Tokyo, Japan. He spent the period 1986–1988 as a research associate at Rice University. His research interests include high-power gas laser devices and their applications.

Dr. Hamada is a member of the Japanese Society of Electrical Engineers.
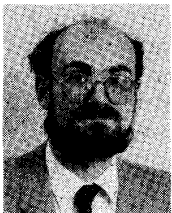
Roland A. Sauerbrey (M'85) was born in Coburg, Germany, on October 28, 1952. He received the M.S. and the Ph.D. degrees, both in physics, from the University of Würzburg, Germany in 1978 and 1981, respectively.

After a year as a postdoctoral fellow at Rice University, Houston, TX, he returned to the University of Würzburg, where he became an Assistant Professor in Physics. In 1985 he joined the faculty of Rice University, where he is presently an Associate Professor with the Department of Electrical and Computer Engineering. His primary research activities have been in the area of short wavelength lasers, as well as excimer spectroscopy and its applications.

Dr. Sauerbrey is a member of the American Optical Society, the American Physical Society, and the German Physical Society.
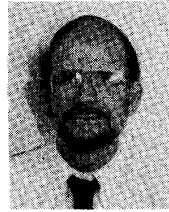
William L. Wilson, Jr. (S'68–M'71–SM'87) was born on February 6, 1943. He received the B.S. degree in 1965, the M.E.E. degree in 1966, and the Ph.D. degree in 1972, all in electrical engineering from Cornell University, Ithaca, NY.

From 1971 to 1972, he was an Instructor-Research Associate with the Electrical Engineering School at Cornell. From 1972 to the present, he has been associated with the Department of Electrical and Computer Engineering at Rice University, Houston, TX, where he now holds the position of Professor. His research interests include tunable excimer lasers and solid-state devices.

Dr. Wilson is a member of Tau Beta Pi, Eta Kappa Nu, Sigma Xi, the IEEE Magnetics Society, the IEEE Microwave Theory and Techniques Society, and IEEE Electron Devices Society, and the American Physical Society.
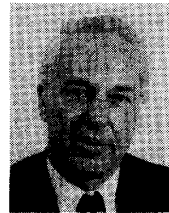
Frank K. Tittel (SM'72–F'86) was born in Berlin, Germany, in 1933. He received the M.A. and Ph.D. degrees from Oxford University, Oxford, England.

From 1959 to 1967, he was a Research Physicist at the General Electric Research and Development Center, Schenectady, NY. Since 1967, he has been at Rice University, Houston, Texas, where he is a Professor in Electrical and Computer Engineering. His research interests include laser devices, laser spectroscopy, and nonlinear optics.

Dr. Tittel is a member of the IEEE Laser and Electro-Optics Society and the American Physical Society, and a Fellow of the Optical Society of America.

William L. Nighan (SM'85) was born in Philadelphia, PA, in 1938. He received the B.S. degree in engineering from the University of Dayton, Dayton, OH, in 1961 and the M.S. degree in engineering science from Northwestern University, Evanston, IL, in 1962.

Since 1962 he has been with United Technologies Research Center, East Hartford, CT, where he is Manager of Applied Physics in the Electronics and Photonics Technologies Department. His primary research activities have been in areas of gas discharge physics, electric lasers, plasma displays, and applied atomic, molecular and chemical physics.

Mr. Nighan is a member of Sigma Xi, Tau Beta Pi, and the American Physical Society.